PIP$_2$ Enrichment

2.5
2.0
1.5
1.0
0.5
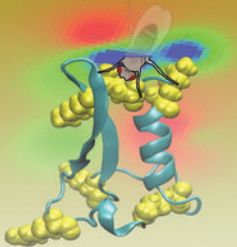
hDAT N-terminus

Phosphatidylinositol (4,5)-bisphosphate regulates psychostimulant behaviors through its interaction with a membrane protein

Peter J. Hamilton[1,9]*, Andrea N. Belovich[2]*, George Khelashvili[3], Christine Saunders[2], Kevin Erreger[4,9], Jonathan A. Javitch[5,6], Harald H. Sitte[7], Harel Weinstein[3,8], Heinrich J.G. Matthies[4,9#], and Aurelio Galli[1,2,4,9#]

[1]Vanderbilt Brain Institute, Departments of [2]Pharmacology, [4]Molecular Physiology & Biophysics, [9]Neuroscience Program in Substance Abuse, Vanderbilt University School of Medicine, Nashville, TN 37232-8548, United States; [3]Department of Physiology and Biophysics, Weill Cornell Medical College of Cornell University, New York, New York 10065, United States; Departments of [5]Psychiatry and [6]Pharmacology, Columbia University College of Physicians & Surgeons, New York, New York 10032, United States; [7]Institute of Pharmacology, Center for Physiology and Pharmacology, Medical University Vienna, Vienna, Austria; [8]HRH Prince Alwaleed Bin Talal Bin Abdulaziz Alsaud Institute of Computational Biomedicine, Weill Cornell Medical College of Cornell University, New York, New York 10065, United States.

Correspondence should be addressed to either of the following: Aurelio Galli, Room 7124, MRB III, or Heinrich J. G. Matthies, Room 7141A, MRB III, E-mail: aurelio.galli@vanderbilt.edu, heinrich.j.matthies@vanderbilt.edu, Vanderbilt University School of Medicine, 465 21st Avenue South, Nashville, TN 37232-8548, USA.

Keywords: dopamine, transporter, amphetamine, *Drosophila melanogaster*, phosphatidylinositol 4,5-bisphosphate

* P.J.H. and A.N.B. contributed equally to this work.

\# H.J.G.M. and A.G. contributed equally to this work.

Phosphatidylinositol (4,5)-bisphosphate (PIP$_2$) regulates the function of ion channels and transporters. Here, we demonstrate that PIP$_2$ directly binds the human dopamine (DA) transporter (hDAT), a key regulator of DA homeostasis and a target of the psychostimulant amphetamine (AMPH). This binding occurs through electrostatic interactions with positively charged hDAT N-terminal residues and is shown to facilitate AMPH-induced, DAT-mediated DA efflux and the psychomotor properties of AMPH. Substitution of these residues with uncharged amino acids reduces hDAT-PIP$_2$ interactions and AMPH-induced DA efflux, without altering the hDAT physiological function of DA uptake. We evaluated, for the first time, the significance of this interaction *in vivo* using locomotion as a behavioral assay in *Drosophila melanogaster*. Expression of mutated hDAT with reduced PIP$_2$ interaction in *Drosophila* DA neurons impairs AMPH-induced locomotion without altering basal locomotion. We present the first demonstration of how PIP$_2$ interactions with a membrane protein can regulate the behaviors of complex organisms.

INTRODUCTION

The functional regulation of plasma membrane proteins by lipid molecules is an integral component of cell function and metabolism[1,2]. Phosphatidylinositol (4,5)-bisphosphate (PIP$_2$) is the phospholipid precursor of the second messengers inositol trisphosphate (IP$_3$), diacylglycerol (DAG), and phosphatidylinositol (3,4,5)-trisphosphate (PIP$_3$), and is, itself, capable of acting as a second messenger and cofactor for regulating protein function[1,3-6]. Additionally, PIP$_2$ has been shown to modulate, through electrostatic interactions, the *in vitro* function of ion channels and transporters, including the serotonin transporter (SERT)[1,7]. A sizeable research effort has been dedicated to determining the diversity of cellular roles for PIP$_2$ and defining the ubiquity of

its electrostatic interactions with various plasma membrane proteins, but how these interactions might modulate the behaviors of complex organisms *in vivo* has never been studied.

The plasma membrane dopamine (DA) transporter (DAT) is a presynaptic protein that plays a pivotal role in regulating DA neurotransmission by mediating the high-affinity reuptake of synaptically-released DA. Gene knockout experiments in multiple organisms, including *Drosophila melanogaster*[8,9], point to the DAT as the main target for the locomotor stimulatory effects of amphetamine (AMPH)[10]. AMPH's addictive properties are mediated, at least in part, through elevation of extracellular DA by inducing DA efflux through the DAT[11,12]. Thus, in order to target and limit AMPH actions pharmacologically, it is essential to understand how to precisely manipulate the DAT to prevent DA efflux without altering its physiological function of DA uptake.

The DAT N-terminus is a structural domain of functional significance. AMPH targets the N-terminus to cause posttranslational modifications (e.g. phosphorylation[13]), which are essential for AMPH to cause DA efflux[14,15] and behaviors[8]. Notably, DAT localization to plasma membrane lipid rafts is also vital for DA efflux[16] and AMPH-induced behaviors[8]. In this study, we elucidate how plasma membrane PIP$_2$, which is enriched in lipid rafts[17,18], dictates specific aspects of the transport cycle through its interactions with the N-terminus of the DAT. In terms of AMPH-induced DA efflux, our experimental and computational data demonstrate that the regulatory effect of PIP$_2$ stems from its electrostatic association with the N-terminus. Here, we introduce the first animal model (*Drosophila melanogaster*) in which we evaluate the behavioral consequences of altered PIP$_2$ interactions with a plasma membrane protein. We reveal that DAT-PIP$_2$ interactions are required for AMPH-induced behaviors, thereby presenting PIP$_2$ and its synthetic pathway as novel regulators of AMPH abuse.

RESULTS

Targeting the psychomotor properties of AMPH with pharmacological approaches requires an understanding of the signaling molecules and DAT structural domains that underlie the ability of AMPH to cause disruption in DA neurotransmission. In this study, we demonstrated that PIP$_2$ interacts with positively charged residues of the DAT N-terminus to define AMPH behaviors.

DAT associates with PIP$_2$

The diversity of cellular roles identified for PIP$_2$ as a signaling molecule targeting ion channels and transporters[1,2] makes PIP$_2$ a strong candidate for regulation of the plasma membrane DAT. In this study, we aimed to determine the modalities of the regulatory function of PIP$_2$ in terms of DA homeostasis and AMPH actions. We demonstrated that human DAT (hDAT) interacts with PIP$_2$ and that this interaction regulates DAT function and DAT associated behaviors. Here, we provide evidence to support the association of DAT with PIP$_2$. First, using live confocal imaging, we show that in hDAT cells, GFP-hDAT (green) co-localized (yellow) with a plasma membrane PIP$_2$ sensor (red) (Fig. 1a). As a PIP$_2$ sensor, we used the pleckstrin homology (PH) domain from phospholipase C$_\delta$ (PHPLC$_\delta$-mRFP) that binds specifically to PIP$_2$ at the plasma membrane and has been used to monitor pools of PIP$_2$[19]. In these cells, we further probed the association of hDAT with PIP$_2$ by immunoprecipitating (IP) PIP$_2$ with an anti-PIP$_2$ antibody and immunoblotting the immunoprecipitates for DAT (IB) with an anti-DAT antibody (see below). These data strongly suggest that PIP$_2$ associates with hDAT in cell lines. To reveal the association between PIP$_2$ and DAT in brain tissue, immunoprecipitations were performed from the striatal tissue of wild-type mice (WT; in presence (+) or absence (-) of the anti-PIP$_2$ antibody) or DAT knock out (KO) mice[10] (Fig. 1b). In contrast to WT mice, DAT-PIP$_2$ association was lacking in DAT KO mice. Moreover, in the absence (-) of the PIP$_2$ antibody, no immunoreactivity was detected. These data demonstrate that PIP$_2$ associates with the DAT both in cell culture

and *ex vivo*.

Liposomal pull-downs reveal a direct interaction between the DAT N-terminus and PIP$_2$

PIP$_2$ is negatively charged at physiological pH[20]. Electrostatic interactions between PIP$_2$ and target proteins are thought to lead to changes in protein conformation and, subsequently, their activity[1,21]. It is recognized that PIP$_2$ binds positively charged (basic) residues, such as Arg and Lys, possibly in proximity to one or more hydrophobic amino acids[1]. Recently, residues K352 and K460 of the SERT (a DAT homolog) have been identified *in vitro* as possible sites that mediate SERT-PIP$_2$ association[7]. In the DAT, the homologous amino acids to K352 and K460 are Lys at position 337 (K337) and Arg at position 443 (R443). We reasoned that these two DAT residues represent possible PIP$_2$ binding sites of functional significance. However, charge-neutralizing substitution of K337 and R443 to Ala (hDAT K337A-R443A), to prevent the interaction of these residues with PIP$_2$, caused substantial trafficking of the DAT away from the plasma membrane, as assessed by cell surface biotinylation. The amount of hDAT K337A-R443A at the cell surface was reduced by 82.6 ± 5.2% (p ≤ 0.01 by Student's t-test; n = 7) with respect to hDAT. Therefore, in DAT, in contrast to SERT, these two residues support DAT surface expression, preventing us from determining whether their possible interaction with PIP$_2$ regulates any mechanistic aspect of the transport cycle.

The N-terminus of the DAT is a structural domain that has been shown to regulate specific aspects of DAT transport cycle, without altering DAT surface expression[14,15,22]. It also contains several Lys and Arg residues (Supp. Fig. 1). We therefore sought to determine whether the N-terminus of the DAT directly interacts with PIP$_2$ *in vitro*. To this end, we generated a purified recombinant GST-fused N-terminal DAT fragment comprising the first 64 N-terminal amino acids of hDAT (GST-64 hDAT)[23]. The lipid binding analysis of the GST-fusion proteins was conducted using liposomes composed of mixed lipids (phosphatidylcholine, either with or

without PIP$_2$) as described in Varnai *et al.*[24]. The GST fusion proteins bound to liposomes were pelleted (liposome-pull down) and the binding was assessed by immunoblotting (anti-GST antibody). Figure 2a (top) shows the pull down of GST fusion proteins (GST and GST-64 hDAT) by liposomes containing (**+**) PIP$_2$, as compared to liposomes lacking (**-**) PIP$_2$. The presence (**+**) or absence (**-**) of PIP$_2$ did not alter pull down of GST alone (GST control). As an additional control, we "sequestered" PIP$_2$ by preincubating the liposomes with a basic peptide consisting of the sequence of the putative PIP$_2$ binding domain of the Kv7.2 channel fused to the fatty acid moiety, palmitic acid[25] (pal-HRQKHFEKRR; positively charged at physiological pH)[25]. This peptide is known to interact electrostatically with the polar head groups of PIP$_2$ to hinder its interaction with plasma membrane proteins[25]. Preincubation of PIP$_2$-containing liposomes with 3 μM of the basic peptide (pal-HRQKHFEKRR) inhibited pull down of GST-64 hDAT. Figure 2a (bottom) shows quantitation of immunoblots obtained from multiple experiments. Comassie stain was utilized to verify equal loading. These *in vitro* data provide the first evidence of a direct interaction between PIP$_2$ and a specific region of a neurotransmitter transporter, the DAT N-terminus.

A detailed structural context of hDAT N-terminal association with PIP$_2$ emerges from computational modeling

To obtain molecular level structural insights into hDAT N-terminal interactions with PIP$_2$-containing membranes, we used a previously described homology model of the hDAT[26-28]. To this we have added a recently constructed model of the DAT N-terminus obtained from a combination of structure-prediction methods (Rosetta, Modeller) and atomistic molecular dynamics (MD) simulations (see Methods). These *in silico* modeling steps enabled the prediction of 3-dimensional folds of the loop segment composed of hDAT residues 1-59 in the context of the complete transmembrane domain. The resulting hDAT model was used in mean-field-level calculations (SCMFM) to quantify the electrostatic interaction of the N-terminus with

PIP_2-enriched lipid membranes.

The dominant role of the electrostatic component of the interaction energy between the hDAT N-terminus and PIP_2-containing membranes was substantiated by the electrostatic potential isosurfaces (EPIs) surrounding the molecular model of the hDAT N-terminal segment shown in figure 2b. The belt-like arrangement of the Lys/Arg residues generates a region of strong positive electrostatic potential (in blue) that favors strong interaction with the negatively charged PIP_2 lipids. Docking this face of the N-terminus to the membrane model and solving for the steady state distributions of the charged lipid species (PIP_2) under the influence of the electrostatic forces it generates[29-31] produces a quantitative estimate of the electrostatic component of the interaction energy. Thus, the rearrangement of the PIP_2 lipids in the electrostatic field of the N-terminal segment is predicted to result in a significantly increased concentration of PIP_2 near the Lys/Arg belt (Fig. 2c, color coding on the membrane shows the segregation of PIP_2 (blue) to be 2.5 times larger than the PIP_2 ambient concentration (yellow/green)). Particularly notable is the strength of the PIP_2 interaction mediated by DAT residues Lys3 and Lys5. Together, these *in silico* studies suggest that the interactions between the hDAT N-terminus and PIP_2 lipids are driven by electrostatic forces.

Disrupting the DAT-PIP₂ interaction inhibits reverse transport of DA

We hypothesized that the functional consequence of DAT-PIP_2 interaction is to support reverse transport of DA. Thus, we disrupted DAT-PIP_2 associations in hDAT cells while recording AMPH-induced DA efflux with amperometry. The amperometric electrode, a carbon fiber electrode juxtaposed to the cell membrane, measures DA efflux by oxidation/reduction reactions, with DA efflux represented as a positive current. To simultaneously record DA efflux while delivering compounds to the intracellular milieu, we combined <u>a</u>mperometry with the whole cell <u>p</u>atch <u>c</u>lamp (APC) technique[9,14]. The whole cell patch electrode controls the

intracellular ionic composition, which includes DA[14] (see Methods).

First, we perfused hDAT cells through the whole cell electrode with DA and the basic peptide pal-HRQKHFEKRR (positively charged at physiological pH and tethered to the plasma membrane through the fatty acid moiety, palmitic acid[25]) while recording DA efflux with the amperometric electrode (Fig. 3a). We used this peptide to compete against the DAT N-terminus for PIP$_2$ interactions as determined in Fig. 2a. Pal-HRQKHFEKRR (3 µM, 10 minutes of intracellular perfusion) was effective in reducing AMPH-induced DA efflux with respect to the efflux obtained with the control peptide pal-HAQKHFEAAA, in which four positive residues were substituted with Ala (Fig. 3a, top). Quantitation of the peak amperometric currents demonstrates that intracellular perfusion of pal-HRQKHFEKRR significantly reduced DA efflux (Fig. 3a, bottom). These data underscore the importance of DAT-PIP$_2$ interactions in the regulation of DA efflux and point to the type of interactions as electrostatic in nature. We next assessed whether DAT-PIP$_2$ association regulates other DAT functions (e.g. DAT-mediated inward currents). We recorded hDAT-mediated inward currents from hDAT cells voltage clamped at -60 mV with a whole-cell electrode containing either pal-HRQKHFEKRR or the control peptide pal-HAQKHFEAAA (3 µM, 10 minutes of intracellular perfusion). We stimulated the hDAT-mediated currents by perfusion of either 10 µM AMPH or DA, respectively. In contrast to DA efflux, pal-HRQKHFEKRR failed to inhibit hDAT-mediated inward currents, with respect to the control peptide, either for AMPH (109 ± 4.9% of control; $p \geq 0.8$ by Student's t-test; n = 4) or for DA (98 ± 16% of control; $p \geq 0.9$ by Student's t-test; n = 4).

To further investigate the role of DAT-PIP$_2$ interactions in AMPH regulation of DAT function, we transfected hDAT cells with the human muscarinic acetylcholine (ACh) receptor M1 (hM1R), a Gαq coupled receptor. Activation of hM1R activates phospholipase C (PLC), stimulating hydrolysis of PIP$_2$ and effectively depleting PIP$_2$ stores[3]. Live imaging was adopted utilizing mRFP tagged PLC-δ1 PH domain (see Fig. 1a) to detect changes of PIP$_2$ levels at the plasma

membrane induced by ACh, a potent hM1R agonist[32]. In hDAT cells, 5 minutes of ACh (100 µM) decreased surface RFP tagged PLC-δ1 PH domain levels to 64 ± 9% of vehicle control (p ≤ 0.009 by Student's t-test comparing ACh to vehicle; n = 16). In cells loaded with DA (see Methods), we next quantified the magnitude of AMPH-induced DA efflux before and after bath perfusion of ACh (5 minutes, 100 µM) (Fig. 3b, top). Quantitation of the change in AMPH-induced DA efflux induced by PIP₂ depletion within the same cell (Fig. 3b, bottom) demonstrates that ACh exposure significantly decreased DA efflux. This decrease was not due to a trafficking phenomenon, since exposure of ACh (5 minutes, 100 µM) in hM1R-expressing hDAT cells did not cause significant trafficking of hDAT away from the plasma membrane as compared to vehicle-treated control (Supp. Fig. 2). We next determined whether providing an excess of intracellular PIP₂ reduces the ability of hM1R agonism to decrease DA efflux. For this, we adopted the APC technique[9,14]. Inclusion of PIP₂ (50 µM) in the whole cell patch pipette solution (10 minutes of intracellular perfusion) impaired the ability of ACh (5 minutes, 100 µM) to significantly decrease AMPH-induced DA efflux with respect to vehicle control (Supp. Fig. 3). Collectively, these data demonstrate that impairing the electrostatic interaction between PIP₂ and DAT selectively inhibits the ability of AMPH to cause DA efflux.

N-terminal lysine residues mediate DAT-PIP₂ association

Since our *in silico* modeling of the hDAT N-terminus indicated residues Lys3 and Lys5 to be essential in facilitating the electrostatic interaction of PIP₂ with DAT (Fig. 2c), we hypothesized that substitution of these residues with uncharged amino acids (e.g. alanine or asparagine) would disrupt DAT-PIP₂ associations. To probe this inference *in silico*, Lys3 and Lys5 were both substituted computationally with either Ala (hDAT K/A) or with Asn (hDAT K/N), and the resulting constructs (N-terminus of hDAT K/A and hDAT K/N) were evaluated for any conformational rearrangements due to the mutations. The constructs were used in the same computational protocols described for the hDAT model. The results for the mutant constructs

show significantly reduced electrostatic interactions with PIP$_2$-containing membranes for both hDAT K/A (Fig. 4a, compare to Fig. 2c) and hDAT K/N (Supp. Fig. 4, compare to Fig. 2c).

 The inferences from the computational evaluation of the N-terminus association with PIP$_2$ lipids *in silico* were probed biochemically by determining the effect of charge neutralizing mutations of Lys3 and Lys5. In hDAT K/A cells, we immunoprecipitated PIP$_2$ and immunoblotted the immunoprecipitates for DAT (IB: anti-DAT). The amount of DAT recovered in the PIP$_2$ immunoprecipitates was reduced in the hDAT K/A cells compared to the hDAT cells (Fig. 4b, top lane). In the absence of antibody against PIP$_2$, no signal was detected for DAT in the immunoprecipitates (Fig. 4b, middle lane, IP: beads). The total DAT in the hDAT K/A cells was not decreased with respect to hDAT cells (Fig. 4b, bottom lane; Total DAT). These data demonstrate that substitution of Lys3 and Lys5 decreases DAT-PIP$_2$ interaction, as predicted from the computational modeling. Quantitation of multiple experiments (n = 4) is shown in figure 4b (bottom). Next, we determined whether substitution N-terminal Lys3 and Lys5 to Ala impairs the direct interaction of DAT with PIP$_2$ *in vitro*. We generated a purified recombinant GST-fused N-terminal DAT fragment comprising the first 64 N-terminal amino acids of hDAT with Lys3 and Lys5 substituted to Ala (GST-64 hDAT K/A). The lipid binding analysis of the GST-fusion proteins (either GST-64 hDAT or GST-64 hDAT K/A) was conducted utilizing liposome-pull down as in figure 2. The inset in figure 4b shows the pull down of the GST fusion proteins by liposomes containing PIP$_2$. Quantitation of immunoblots obtained from multiple experiments demonstrated that pull down of GST-64 hDAT was significantly inhibited by Lys to Ala substitution (GST-64 hDAT K/A was 0.45 ± 0.2% of GST-64 hDAT; p ≤ 0.037 by Student's t-test; n = 4).

In order to assess whether DAT physiological function is altered by disrupting DAT-PIP$_2$ association, we examined radioactive [^{3}H]DA uptake in both hDAT and hDAT K/A cells. In hDAT K/A cells, the maximal velocity of DA influx (V_{max}) and the apparent DA affinity (K_m) were not

significantly different from those of hDAT (Fig. 5a, top). A representative plot of DA uptake kinetics (in triplicate) for hDAT and hDAT K/A is shown in Fig. 5a (bottom), demonstrating that the uptake of substrate is not regulated by the interaction with PIP_2. Consistent with the uptake data, no significant difference was found in the whole-cell DAT-mediated inward current (recorded at -60 mV) between hDAT and hDAT K/A cells upon stimulation with 10 μM DA. The hDAT K/A inward currents were expressed as a percent of hDAT-mediated currents ($103 \pm 20\%$ of hDAT; $p \geq 0.97$ by Student's t-test; n = 4).

Our pharmacological manipulations (Fig. 3) indicate that disrupting DAT-PIP_2 association has no effect on DAT-mediated DA uptake or DA-induced inward currents but inhibits the ability of AMPH to cause DA efflux. Consistent with this, hDAT K/A cells were found to display strikingly reduced AMPH-induced DA efflux (Fig. 5b, top). Quantitation of the amperometric recordings demonstrate that the Lys to Ala substitution not only decreased DAT-PIP_2 association (Fig. 4), but also decreased the ability of AMPH to cause DA efflux (Fig. 5b, bottom). The reduced AMPH-induced DA efflux was not associated with a reduction in either total or DAT surface expression as assessed by measuring changes in DAT proteins in the total and biotinylated fraction, respectively. Surface fractions were quantitated, normalized to total DAT, and expressed as a percent of hDAT (hDAT K/A was $122 \pm 31\%$ of hDAT; $p \geq 0.53$ by Student's t-test; n = 7-8). The findings in the hDAT K/A cells were mirrored by those obtained in the hDAT K/N cells in terms of both DAT-PIP_2 association and hDAT cell surface expression (Supp. Fig. 5a and 5b). The hDAT K/N also displayed normal uptake (Supp. Fig. 5c) and, like the hDAT K/A, had a significant reduction in AMPH-induced DA efflux (Supp. Fig. 5d). Furthermore, AMPH uptake assays revealed that hDAT, hDAT K/A, and hDAT K/N cells displayed comparable AMPH transport (see Methods) (hDAT K/A: $101 \pm 4.9\%$ and hDAT K/N: $93.9 \pm 17\%$ relative to hDAT; $p \geq 0.88$ by one-way ANOVA; n = 3, in triplicate). These results demonstrate that the reduced ability of AMPH to cause DA efflux promoted by the Lys to Ala substitutions does not involve changes in the surface expression or changes in ability of the DAT mutants to

transport AMPH. Another possibility for this decrease in DA efflux is that the N-terminal Lys substitution (hDAT K/A) perturbs the potential AMPH-induced phosphorylation of the Ser2 and Ser4 adjacent to these Lys residues by altering primary sequence requirements for phosphorylation. To explore this, we substituted Ser2 and Ser4 with Asp (to mimic phosphorylation) in the hDAT K/A background (hDAT K/A-S/D). Cells expressing hDAT K/A-S/D exhibited significantly reduced AMPH-induced DA efflux, similar to hDAT K/A cells (Supp. Fig. 6a, top). Quantitation of the amperometric recordings demonstrated that Ser to Asp substitution at positions 2 and 4 in the hDAT K/A background did not rescue the ability of AMPH to cause DA efflux (Supp. Fig. 6a, bottom). The reduced AMPH-induced DA efflux was not associated with a reduction in DA uptake (Supp. Fig. 6b). These data demonstrate that the reduction in DA efflux caused by substitution of Lys3 and Lys5 with uncharged amino acids cannot be attributed to impaired phosphorylation of adjacent Ser residues.

Reduced DAT-PIP₂ interaction selectively prevents the psychomotor stimulant effects of AMPH with no changes in circadian locomotor activity

Locomotion is an elemental behavior regulated by DA across species, including *Drosophila melanogaster*[8,9,33,34]. Recently, locomotion in flies has been adopted to evaluate molecular discoveries of AMPH actions mechanistically *in vivo*[8,9]. Thus, *Drosophila* offer a powerful model for elucidating the impact of altered DAT-PIP₂ interactions on locomotion and on the psychomotor stimulant effects of AMPH.

We expressed hDAT or hDAT K/A in flies homozygous for the *Drosophila* DAT null allele, *DAT^fmn* (dDAT KO)[35], by using the Gal4/UAS system to express a single copy of hDAT or hDAT K/A in a *dDAT^fmn* mutant background, selectively in DA neurons[9]. To generate the transgenic flies, we used phiC31-based integration, which leads to the expression of comparable levels of mRNA for the relevant transgenes (hDAT or hDAT K/A). Locomotion was quantified by beam

crossing detection over a >24 hour period (data binned in 15 minute intervals) during both the light (horizontal white bar) and dark (horizontal black bar) cycle. While dDAT KO flies were hyperactive[35], dDAT KO flies expressing hDAT in DA neurons had reduced basal locomotion as compared to dDAT KO (Fig. 6a, compare hDAT to dDAT KO). These data demonstrate the validity of expressing hDAT in *Drosophila* for behavioral studies.

We hypothesized that flies harboring the hDAT K/A would demonstrate comparable locomotion with respect to hDAT expressing flies, since no difference in DA uptake was observed. Figure 6a demonstrates that *Drosophila* expressing hDAT and hDAT K/A displayed comparable basal locomotion, whereas dDAT KO flies exhibited chronically elevated locomotion. Total circadian locomotor activities (24 hour) of hDAT and hDAT K/A flies were not significantly different, while total locomotor activity of dDAT KO flies was significantly higher than hDAT and hDAT K/A (Fig. 6b).

Encouraged by the lack of hyperactivity of hDAT K/A flies under basal conditions, we hypothesized that these flies would have blunted AMPH-induced locomotive behaviors resulting from reduced ability of AMPH to stimulate DA efflux. While AMPH caused a significant increase in locomotion in flies expressing hDAT, this increase was significantly reduced in flies expressing hDAT K/A (Fig. 7a). These data demonstrate, for the first time, the behavioral importance of the interaction of PIP_2 with a plasma membrane protein. This discovery is further enhanced by our ability to associate blunted AMPH-induced behaviors with a decreased ability of AMPH to cause DA efflux in isolated DA neurons from flies expressing hDAT K/A (Fig. 7b). *Ex vivo* cultures of *Drosophila* DA neurons were investigated with amperometry to quantify the magnitude of the AMPH-induced DA efflux in the different fly lines. The DA efflux recorded from hDAT K/A expressing neurons was significantly reduced compared to hDAT expressing neurons (Fig. 7b), suggesting that the reduced AMPH-induced locomotion in flies expressing hDAT K/A is due to diminished DA efflux in response to AMPH.

It is possible that this PIP$_2$ regulation of DA efflux is an evolutionarily conserved mechanism that controls DAT function across phylogeny. To test this possibility, we utilized the APC technique in CHO cells expressing the dDAT (dDAT cells). In dDAT cells, intracellular perfusion of pal-HRQKHFEKRR (3 μM, 10 minutes) was effective in reducing AMPH-induced DA efflux with respect to the efflux obtained with the control peptide pal-HAQKHFEAAA (34.9 ± 12.9% of control peptide; p ≤ 0.01 by Student's t-test; n = 3). These results parallel those obtained in hDAT cells (Fig. 3). In this study, we provide the first behavioral evidence for the relevance of the interaction of PIP$_2$ with a plasma membrane protein, associating AMPH behaviors to altered neuronal DAT function within the same organism.

DISCUSSION

We recently demonstrated that disrupting the localization of DAT in lipid rafts impairs the ability of AMPH to cause both DA efflux (without altering DA uptake)[16], and associated behaviors[8]. This led us to hypothesize that the molecular underpinnings required for AMPH actions reside in lipid rafts. Raft microdomains are considered scaffolds for PIP$_2$ signaling, enabling PIP$_2$ to selectively regulate different cellular processes[36]. Yet, partitioning of PIP$_2$ into lipid rafts has been criticized as energetically improbable, since PIP$_2$ consists of a polyunsaturated acyl side chain (arachidonic acid) that is unlikely to spontaneously partition into cholesterol-rich rafts[20]. Therefore, it is theorized that the partitioning of PIP$_2$ into rafts is facilitated by interactions with raft-localized proteins[20]. Here we demonstrate that PIP$_2$ directly interacts with hDAT, a protein that localizes to the rafts[16,37,38].

We found that the DAT N-terminus (a domain of functional importance)[14,15] is engaged in direct electrostatic interactions with PIP$_2$, described by both computational and biochemical analysis. We demonstrate that this interaction is direct and distinct from the recently described association of PIP$_2$ with SERT[7]. This DAT-PIP$_2$ interaction, which occurs in brain tissue, involves

the two most distal N-terminal Lys (Lys3 and Lys5). These data, combined with the regulatory nature of DAT localization to PIP$_2$ enriched lipid rafts, led us to hypothesize that PIP$_2$ participates in coordinating the complex molecular events underlying *specific* DAT activities. This includes AMPH-induced DA efflux. Notably, this interaction does not regulate the physiological function of DAT (DA uptake), DAT surface expression, and AMPH uptake. Other functions of the DAT include AMPH- or DA-stimulated inward currents that represent inward movements of ions associated with the transport of substrate. Therefore, we expected that substrate-induced inward currents would not be affected by disruption of DAT-PIP$_2$ interaction, in the same way that DA or AMPH uptake is not affected. We show that disrupting DAT-PIP$_2$ interaction by substitution of Lys3 and Lys5 with Ala did not impair the ability of hDAT to sustain electrical inward currents stimulated by either DA or AMPH. The regulatory nature of the direct DAT-PIP$_2$ interaction on DAT-mediated DA efflux is underscored by our results demonstrating that "sequestering" PIP$_2$, with our palmitoyl-positively charged peptide, or depleting PIP$_2$, by stimulating PLC activity, results in diminished reverse transport of DA. Consistent with these findings is the notable result that intracellular perfusion of the palmitoyl-positively charged peptide did not impair hDAT-mediated inward currents stimulated by either AMPH or DA relative to control peptide. These data underscore the interaction between DAT and PIP$_2$ as a key regulator of the specific DAT function of DA efflux.

N-terminal phosphorylation is a requirement for the ability of AMPH to cause a robust DA efflux[14]. The results of our specific molecular manipulations support the notion that Lys to Ala substitution did not impair DA efflux by altering primary sequence requirements for phosphorylation of Ser2 and Ser4. Indeed, pseudophosphorylation of these Ser residues in the hDAT K/A background failed to rescue DA efflux. Consistent with this notion, palmitoyl-positively charged peptide (which does not alter the N-terminus primary sequence) disrupts both the direct interaction of the N-terminus with PIP$_2$ as well as DA efflux. However, the computational modeling reveals the possibility that the strength of the association of Lys3 and Lys5 with PIP$_2$

regulates the proper conformation of the DAT N-terminus and affects the transporter N-terminus as a whole. Therefore, we cannot exclude the possibility that the observed DAT-PIP$_2$ association regulates N-terminal phosphorylation of non-adjacent Ser by coordinating suitable conformations. Nevertheless, this possibility does not diminish the importance of the discovery that DAT-interaction with PIP$_2$ is a key determinant of AMPH-induced DA efflux and behaviors. On the contrary, it highlights an opportunity, in future studies, to understand whether the DAT N-terminal interaction with PIP$_2$ supports N-terminal phosphorylation and/or the importance of phosphorylation for N-terminal conformations and DAT-PIP$_2$ association.

The Ser-Lys-Ser-Lys N-terminal sequence of the DAT is conserved across several species, including *Drosophila*, suggesting that the DAT-PIP$_2$ association is a possible evolutionarily conserved mechanism that regulates specific DAT functions. Our data demonstrate that disruption of the dDAT-PIP$_2$ interaction impairs DA efflux, which parallels our results in the hDAT. It is tempting to speculate that this mechanism of N-terminal regulation of transporter function through electrostatic interactions with PIP$_2$ is a potential mode of regulation for other neurotransmitter transporters as well. Examination of sequences of the N-terminal regions of four major neurotransmitter transporters (hDAT, hSERT, hNET, and hVMAT2) reveals that the positively charged residues are not only abundant in this region, but are also often clustered. In the hDAT, we revealed the consequences of this clustering in a structural context, where one of these clusters contains Lys3 and Lys5, which enables this region to attract PIP$_2$ lipids. Therefore, a mechanism of PIP$_2$ regulation, similar to the one outlined here for DAT function, may apply to other neurotransmitter transporters with charged clusters in their N-terminal sequences.

Recently we discovered that the AMPH-induced 5-HT efflux mediated by SERT also relies on PIP$_2$ interactions with positively-charged residues[7]. However, these residues are not localized to the N-terminus of SERT. These data do not exclude a possible role of SERT N-terminus basic

residues in SERT-PIP$_2$ interaction and AMPH-induced 5-HT efflux. In contrast, in DAT, mutation (to Ala) of the corresponding SERT-PIP$_2$ binding sites causes substantial trafficking of DAT away from the plasma membrane, disrupting its membrane expression. Thus, this trafficking phenomenon prevents our ability to determine the significance of these residues in the mechanistic aspects of the DAT transport cycle. However, it is clear that they do not functionally replace Lys3 and Lys5 in terms of DA efflux.

Prior to this work, it was unclear whether the association and/or dissociation of plasma membrane proteins with PIP$_2$ played a role in the regulation of behaviors of complex organisms. Here, we took advantage of an animal model (*Drosophila melanogaster*) to determine the behavioral consequences of disrupting direct interactions of DAT with PIP$_2$. *Drosophila* expressing hDAT K/A solely in DA neurons did not display altered circadian locomotor activity. This is not surprising, since the cells expressing hDAT K/A have both normal DA uptake and DA affinity. However, hDAT K/A flies exhibit significant reductions in the behavioral psychomotor responses to AMPH. These data convey the significance of the interaction between PIP$_2$ and plasma membrane proteins (i.e. DAT) in fundamental organismal behaviors, such as locomotion. The discovery of this PIP$_2$ regulation of the psychomotor actions of AMPH is further enhanced by our ability to record DA efflux (for the first time) directly from DA neurons cultured from the same *Drosophila* lines utilized in our behavioral assays. DA neurons expressing hDAT K/A have a significant reduction in DA efflux with respect to neurons expressing hDAT. This enhances our molecular discoveries outlining the DAT-PIP$_2$ interaction as required for DA efflux and obligatory in the ability of AMPH to cause psychomotor behaviors. These data promote PIP$_2$ and its synthetic pathway from its canonical role as a modulator of cell function and metabolism to a new role as a regulatory agent of both elemental behaviors, such as locomotion, and maladaptive behaviors, such as psychostimulant abuse.

Abbreviations: dopamine (5-hydroxytryptamine, DA), human dopamine transporter (hDAT), amphetamine (AMPH), Phosphatidylinositol (4,5)-bisphosphate (PIP$_2$)

Competing interests: The authors declare no competing interests.

LEGENDS

Figure 1: PIP$_2$ interacts with hDAT.

(a) hDAT and PIP$_2$ co-localize at the plasma membrane. In hDAT expressing cells, GFP-hDAT (green) co-localizes (yellow) at the plasma membrane with the PIP$_2$ sensor PHPLC$_\delta$-mRFP (red) (representative image from three live experiments with of 10-15 cells imaged per experiment). **(b)** PIP$_2$ associates with endogenous mouse DAT in striatal tissue. In striatal lysate, DAT was detected in PIP$_2$ immunoprecipitates using an anti-DAT antibody (+). DAT immunoreactivity was absent in the beads fraction (-) and in PIP$_2$ immunoprecipitates from DAT knock out (KO) animals (endogenous mouse IgG is observed) (representative of n = 3).

Figure 2: hDAT-PIP$_2$ electrostatic interactions are mediated by the hDAT N-terminus.

(a) hDAT N-terminus binds directly to PIP$_2$. GST-64 hDAT is enriched in liposome-pull downs with liposomes containing PIP$_2$ (+) as compared to liposomes lacking PIP$_2$ (-) (** = p ≤ 0.01 by one-way ANOVA followed by Bonferroni post-hoc test; n = 3). Pull down of GST control was not altered by the presence (+) of absence (-) of PIP$_2$ in the liposomes (p ≥ 0.05 by one-way ANOVA followed by Bonferroni post-hoc test; n = 3). Preincubation of liposome containing PIP$_2$ with 3 µM of pal-HRQKHFEKRR (+) inhibited the pull down of GST-64 hDAT with liposomes

containing PIP$_2$ (** = p ≤ 0.01 by one-way ANOVA followed by Bonferroni post-hoc test; n = 3).

(b) Electrostatic potential (EP) isosurfaces (+1kT/e (+ charge)) shown as *blue wireframes* and (-1kT/e (- charge)) as *red wireframes* calculated for the predicted structure of the wild type N-terminus. **(c)** View from the intracellular side of the N-terminus (model) adsorbing on the lipid membrane. For clarity, the orientation of the N-terminus in panel (c) was obtained by a 180° rotation of the N-terminus configuration shown in panel (b). The level of the PIP$_2$ segregation by the N-terminus is expressed as the ratio of local and ambient lipid fraction values, and illustrated in color code (cold colors represent an enrichment of PIP$_2$). The positive residues in the N-terminus (yellow) that attract PIP$_2$ electrostatically are highlighted.

Figure 3: Sequestration or depletion of PIP$_2$ inhibits AMPH-induced DA efflux.

(a) Sequestering PIP$_2$ with pal-HRQKHFEKRR decreases AMPH-induced DA efflux. Top: representative traces from stably transfected hDAT cells after patch delivery of 3 µM control peptide (pal-HAQKHFEAAA) or PIP$_2$ sequestering peptide (pal-HRQKHFEKRR) to the cytoplasm of the cell. Arrows indicate the application of 10 µM AMPH. Bottom: quantitation of amperometric peak currents for the two different treatments. Data are expressed as percentage of vehicle control (*** = p ≤ 0.0001 by Student's t-test; n = 7). **(b)** Depleting PIP$_2$ levels reduces AMPH-induced DA efflux. Top: representative trace of responses to 1 µM AMPH in stably transfected hDAT cells, co-expressing the human muscarinic acetylcholine receptor 1 (hM1R), before and after exposure to 100 µM acetylcholine (ACh). Bottom: quantitation of the amperometric peak currents representing AMPH-induced DA efflux before and after ACh-dependent PIP$_2$ depletion (* = p ≤ 0.05 by Student's t-test; n = 11).

Figure 4: hDAT N-terminal Lys regulate hDAT-PIP$_2$ interaction.

(a) Mutating hDAT N-terminal residues Lys3 and Lys5 to uncharged Ala (hDAT K/A) disrupts PIP$_2$ segregation to the N-terminus. View from the intracellular side of the N-terminus of hDAT K/A adsorbing on the lipid membrane. The level of PIP$_2$ segregation by the N-terminus residues

is expressed as the ratio of local and ambient lipid fraction values and illustrated in color code, with cold colors representing an enrichment of PIP_2. **(b)** N-terminal Lys residues mediate hDAT-PIP_2 interaction. Top: PIP_2 immunoprecipitates from hDAT and hDAT K/A cells were immunoblotted for DAT (top lane). The beads fraction supports absence of non-specific binding (middle lane). Bottom lane shows total DAT proteins. Bottom: quantitation of PIP_2 pulldown band intensities normalized to the respective total DAT and expressed as a percentage hDAT (*** = $p \leq 0.001$ by Student's t-test; n = 4). *Inset:* Representative blot for GST-64 hDAT and GST-64 hDAT K/A in pull downs with liposomes containing PIP_2.

Figure 5: N-terminal Lys3 and Lys5 regulate specific modalities of hDAT function.

(a) hDAT K/A exhibits normal DA uptake function. Top: kinetic parameters (V_{max} and K_m) for hDAT and hDAT K/A (V_{max}: $p \geq 0.92$ by Student's t-test; n = 3, in triplicate; K_m: $p \geq 0.62$ by Student's t-test; n = 3, in triplicate). Bottom: representative plot of [³H]DA uptake kinetics in hDAT (filled squares) and hDAT K/A (empty squares) cells ($p \geq 0.05$, by two-way ANOVA followed by Bonferroni post-test; in triplicate). **(b)** hDAT K/A has reduced AMPH-induced DA efflux. Top: representative AMPH-induced amperometric currents recorded from hDAT and hDAT K/A cells. Arrows indicate application of 10 µM AMPH. Bottom: quantitation of AMPH-induced DA efflux. Data are represented as maximal DA efflux expressed as percent of the DA efflux recorded in hDAT controls (* = $p \leq 0.05$ by Student's t-test; n = 7-8).

Figure 6: Expression of hDAT K/A in *Drosophila* dopaminergic neurons does not affect circadian locomotor activity.

hDAT or hDAT K/A was expressed in DA neurons of dDAT KO flies. **(a)** Locomotor activity was assayed over 32 hours during the light (horizontal white bars) or dark (horizontal black bars) cycle. Flies expressing dDAT KO flies (blue squares) were hyperactive throughout the 32 hour period with respect to flies expressing wild type hDAT (black squares) as well as flies expressing hDAT K/A (red squares) (beam breaks binned in 15 minute intervals; n = 31-42). **(b)**

Quantitation of total beam crosses over 24 hours for hDAT, hDAT K/A, and dDAT KO flies (*** = p ≤ 0.001 by one-way ANOVA followed by Bonferroni post-test; n = 31-42).

Figure 7: Expression of hDAT K/A in *Drosophila* dopaminergic neurons impairs AMPH-induced locomotion and DA efflux in DA neurons.

(a) hDAT K/A expressing flies have blunted locomotor responses to AMPH. Changes in locomotion were determined upon AMPH or vehicle exposure over 15 minutes and calculated as beam crosses. AMPH did not cause a significant increase in locomotion in hDAT K/A flies compared to vehicle control (p ≥ 0.05 by one-way ANOVA followed by Bonferroni post-test; n = 25-49). This is in contrast to flies expressing hDAT, where AMPH induced a significant increase in locomotion compared to vehicle control (*** = p ≤ 0.001 by one-way ANOVA followed by Bonferroni post-test; n= 25-60). **(b)** hDAT K/A *Drosophila* DA neurons show reduced AMPH-induced DA efflux. Dopaminergic neurons were selected by fluorescence microscopy in which the expression of mCherry is driven by TH-GAL4. Representative AMPH-induced amperometric currents recorded from hDAT and hDAT K/A expressing DA neurons. Arrows indicate application of 1 μM AMPH. Bottom: quantitation of total AMPH-induced DA efflux. Data are represented as cumulative DA efflux expressed as percent of the DA efflux recorded in hDAT neurons (** = p ≤ 0.01 by Student's t-test; n = 4-5).

Supplementary Figure 1:

Sequences of the N-terminal regions of the human dopamine transporter (hDAT), serotonin transporter (hSERT), norepinephrine transporter (hNET), and vesicular monoamine transporter 2 (hVMAT2); positively charged residues are represented in red.

Supplementary Figure 2:

Representative immunoblots for biotinylated (surface) and total hDAT protein fractions from stably transfected hDAT cells, co-expressing the human muscarinic acetylcholine receptor 1

(hM1R), treated either with vehicle or 100 µM ACh for 5 min. Surface fractions were quantitated, normalized to total hDAT, and expressed as a percent of vehicle treated hDAT cells ($p \geq 0.7$ by Student's t-test; n = 3 in duplicate).

Supplementary Figure 3:

Excess of intracellular PIP₂ levels prevents the ability of ACh to decrease AMPH-induced DA efflux. Top: representative traces of AMPH responses obtained with the APC technique in stably transfected hDAT cells, co-expressing hM1R, perfused intracellularly with 50 µM PIP₂. Cells were pre-exposed to either 100 µM ACh or vehicle for 5 minutes and DA effluxes induced by 10 µM AMPH were recorded in the continuous presence of ACh or vehicle. Bottom: quantitation of the amperometric peak currents normalized to vehicle control, and expressed as a percent of vehicle treated hDAT cells ($p \geq 0.9$ by Student's t-test; n = 4).

Supplementary Figure 4:

Mutation of hDAT N-terminal residues Lys3 and Lys5 to uncharged Asn (hDAT K/N) disrupts PIP₂ segregation to the N-terminus. View from the intracellular side of the N-terminus of hDAT K/N adsorbing on the lipid membrane. The level of PIP₂ segregation by the N-terminus is expressed as the ratio of local and ambient lipid fraction values, and illustrated in color code with cold colors representing an enrichment of PIP₂.

Supplementary Figure 5:

(a) Top: PIP₂ immunoprecipitates from hDAT and hDAT K/N cells were immunoblotted for DAT (top lane). The beads fraction supports absence of non-specific binding (middle lane). Bottom lane shows total DAT proteins. Bottom: quantitation of PIP₂ pull down band intensities normalized to the respective total DAT and expressed as a percentage hDAT (*** = $p \leq 0.0001$ by Student's t-test; n = 3). **(b)** Representative immunoblots for biotinylated (surface) and total protein fractions from hDAT and hDAT K/N cells. Immunoblots for surface NaK-ATPase and

total ERK are shown as well. Surface fractions were quantitated, normalized to total DAT, and expressed as a percentage of hDAT (p ≥ 0.41 by Student's t-test; n = 4-5). **(c)** [H^3]DA uptake (50 nM) in hDAT and hDAT K/N cells was expressed as a percent of uptake in hDAT cells (p ≥ 0.16 by Student's t-test; n = 3, in quadruplicate). **(d)** Representative AMPH-induced amperometric currents recorded from hDAT and hDAT K/N cells. Arrows indicate application of 10 μM AMPH. Bottom: quantitation of AMPH-induced DA efflux. Data are represented as maximal DA efflux expressed as a percent of the DA efflux recorded in hDAT cells (* = p ≤ 0.02 by Student's t-test; n = 6-7).

Supplementary Figure 6:

 (a) hDAT K/A-S/D has reduced AMPH-induced DA efflux. Top: representative AMPH-induced amperometric currents recorded from hDAT and hDAT K/A-S/D cells. Arrows indicate application of 10 μM AMPH. Bottom: quantitation of AMPH-induced DA efflux. Data are represented as maximal DA efflux expressed as a percent of DA efflux recorded in hDAT cells (* = p ≤ 0.03 by Student's t-test; n = 5-6). **(b)** hDAT K/A-S/D exhibits normal [H^3]DA uptake (50 nM) function. Data expressed as a percent of the uptake measured in hDAT cells (p ≥ 0.2 by Student's t-test; n = 4-8).

ONLINE METHODS

Cell culture and transfection. The GFP-hDAT-pCIHygro expression vectors containing hDAT, hDAT K/A (Lys3 and Lys5 to Ala), hDAT K/N (Lys3 and Lys5 to Asn), or hDAT K/A-S/D (Lys3 and Lys5 to Ala and Ser2 and Ser4 to Asp) sequence were generated, confirmed and transiently transfected into Chinese hamster ovary (CHO) cells. The *Drosophila* DAT cDNA was generously provided by the laboratory of Dr. Satinder Singh (Yale University). In some experiments (noted in figure legend), stably transfected hDAT CHO cells were used. These cells were generated as described in Bowton *et al.*[22]. Cells were maintained in a 5% CO_2 incubator at

23

37°C and maintained in Ham's F-12 medium supplemented with 10% fetal bovine serum (FBS), 1 mM L-glutamine, 100 U/mL penicillin, and 100 µg/mL streptomycin. Stably transfected hDAT CHO cells were kept under selection with 250 µg/mL hygromycin B (Corning Cellgro). Fugene-6 (Roche Molecular Biochemicals) in serum-free media was used to transfect cells using a 6:1 transfection reagent:DNA ratio. Assays were conducted 24-48 hours post transfection.

Drosophila neuron culture. Drosophila neurons were cultured from 1-3 day old males. Brains were dissected in Schneider's medium with 1.5% bovine serum albumen (BSA) and optic lobes were removed. Brains were washed with Schneider's medium and incubated for 40 minutes in collagenase (0.3%) and trypsin (0.125%). They were washed in Schneider's medium supplemented with 10% heat inactivated FBS. Dissociated cells were obtained by brain trituration in medium. Cells from each brain were plated on one poly-D-lysine coated MatTek® dish treated with collagen (type IV). Assays were performed the next day.

Cell imaging. We used the pleckstrin homology (PH) domain from phospholipase C$_δ$ (PHPLC$_δ$-mRFP) that binds to PIP$_2$ at the plasma membrane and has been used to monitor pools of PIP$_2$ at the plasma membrane[19]. Cells on poly-D-lysine coated MatTek® dishes were co-transfected with GFP-DAT and PHPLCδ-mRFP and, after 48 hours, were deprived of serum overnight. Single confocal image sections were generated by using a LSM 510 inverted confocal microscope (Zeiss) by sequential imaging of live cells.

Co-immunoprecipitations. Cells were grown to confluence in 25 cm^2 culture flasks and serum deprived overnight prior to assay. On the day of the assay, cells were washed three times with 4˚C phosphate-buffered saline (Gibco) containing 1 mM EGTA and 1 mM EDTA and lysed in RIPA buffer (100 mM NaCl, 1.0% IGEPAL CA-630 (NP-40), 0.5% sodium deoxycholate, 0.1% SDS, 50 mM Tris, pH = 8.0, supplemented with a protease inhibitor cocktail (Sigma Aldrich)). Lysates were passed twice through a 27.5 gauge needle and centrifuged at 15,000 x g for 30

minutes. With a portion of the total cell lysate (TCL) collected to run as the totals, 1 mL of the remaining supernatant was incubated at 4°C for 4 hours with Sepharose-G beads (Fisher Scientific), previously washed with 1% BSA in RIPA buffer and preincubated with 2.5 µg PIP$_2$ antibody (mouse monoclonal, Enzo Life Sciences). For the negative control, TCL supernatant was incubated with BSA-blocked Sepharose-G beads alone. Beads were spun down, washed with cold RIPA buffer, and samples eluted with Laemmli sample buffer at 95°C for 5 minutes. TCL and eluates were analyzed by SDS-PAGE and immunoblotting (see below for antibody details). Band intensity was quantified using ImageJ software (National Institutes of Health). The association between PIP$_2$ and hDAT variants was represented as the ratio of eluate:TCL band intensity, normalized to the eluate:TCL ratio observed in hDAT and expressed as a percent. For the mouse DAT-PIP$_2$ co-immunoprecipitations from striatum, the same protocol was used with the following modifications: striatum was dissected from either wild-type or DAT KO mice, solubilized in RIPA buffer (1:10 weight/volume), homogenized, lysed on ice for 30 minutes and then centrifuged. The remaining protocol was performed as described above.

Cell surface biotinylation and protein immunoblot. Cells were cultured in 6-well plates. For cell surface biotinylation assays, cells were labeled with sulfo-NHS-SS-biotin (1.0 mg/ml; Pierce) before purification and analysis via SDS-PAGE/immunoblots[39]. hDAT was detected using a rat monoclonal primary antibody to the N-terminus of hDAT (1:1000) (Millipore Bioscience Research Reagents) and a goat-anti-rat-HRP-conjugated secondary antibody (1:5000; Jackson ImmunoResearch).

Gluthathione transferase (GST) fusion proteins. GST and GST fused to the first 64 N-terminal amino acids of hDAT were purified as in Binda *et al.*[23] with some modifications. Briefly, GST and the GST fusion proteins were produced in *Escherichia coli* BL21 DE3 LysS. The culture was grown at 30°C, expression induced by the addition of 1 mM isopropylβ-d-1-thiogalactopyranoside at 18°C, and the culture was harvested 8 hours after induction. The

frozen pelleted bacteria was thawed in Tris-buffered saline (TBS) containing 10% glycerol and a Bacterial Protease inhibitor cocktail (Roche Diagnostics)(pH 7.4) and treated with 1 mg/mL lysozyme followed by 15 mM CHAPS. It was then sonicated and cleared by centrifugation. The lysate was passed over glutathione Sepharose 4B beads (GE Healthcare) and washed several times with TBS, followed by 10 mM Tris containing 10% glycerol and eluted with TBS containing 10 mM gluthathione. The quality, size, and amount (relative to BSA) of GST fusions were determined by SDS-PAGE and Bio-Safe Coomassie G-250 Stain. The amount was determined by analysis of imaged gels using ImageQuantTL.

Liposome binding. GST and GST fusion proteins where incubated with or without liposomes for 10 minutes at room temperature, centrifuged at 100,000 x g for 20 minutes at 4°C, and analyzed by immunoblot analysis using anti-GST antibodies (The Vanderbilt Antibody and Protein Resource Core). Liposomes were formed by extrusion of synthetic lipids at a final concentration of 1 mM. Liposomes were formed in 10 mM HEPES/TRIS, 100 mM NaCl with 95% phosphatidylcholine (DOPC; Echelon) and 5% PIP₂ (Phosphatidylinositol 4,5-bisphosphate diC16) at a pH of 7.4.

Amperometry and patch clamp electrophysiology. Cells were plated at a density of ~20,000 per 35-mm culture dish. To preload cells with DA, dishes were washed with KRH assay buffer (130 mM NaCl, 1.3 mM KCl, 1.2 mM KH_2PO_4, 10 mM HEPES, and 2.2 mM $CaCl_2$, pH 7.4) containing 10 mM dextrose, 100 µM pargyline, 1 mM tropolone, and 100 µM ascorbic acid, and incubated with 1 µM DA in KRH assay buffer for 20 minutes at 37°C. To preload *Drosophila* neurons, dishes were washed with KRH assay buffer (as above) containing 100 nM raclopride, and incubated with 1 µM DA in KRH assay buffer for 20 minutes at 26°C. All dishes were washed three times with the external bath solution (130 mM NaCl, 10 mM HEPES, 34 mM dextrose, 1.5 mM $CaCl_2$, 0.5 mM $MgSO_4$, 1.3 mM KH_2PO_4, adjusted pH to 7.35, and 300 mOsm).

To deliver DA (2 mM, Sigma Aldrich), PIP$_2$ inhibitory/control peptides (3 µM pal-HRQKHFEKRR or pal-HAQKHFEAAA), and/or PIP$_2$ (50 µM, phosphatidylinositol 4,5-bisphosphate diC8, Echelon Biosciences), a programmable puller (model P-2000, Sutter Instruments, Novato CA) was used to fabricate quartz recording pipettes with a resistance of 3-5 MΩ. These pipettes were filled with an internal solution containing: 120 mM KCl, 10 mM HEPES, 0.1 mM CaCl$_2$, 2 mM MgCl$_2$, 1.1 mM EGTA, 30 mM dextrose, pH 7.35, and 275 mOsm. Upon gaining access to the cells, the internal solution was allowed to diffuse into the cell for 10 minutes.

Experiments involving perfusion of AMPH or DA (Fig. 3b and inward current experiments) utilized double-barrel quartz tubing with an inner diameter of 250 µm (Polymicro Technologies, Phoneix AZ) placed ~80 µm from the cell. DAT-mediated inward currents were recorded at -60 mV.

To record DA efflux, a carbon fiber electrode (ProCFE; fiber diameter of 5 µm; obtained from Dagan Corporation) juxtaposed to the plasma membrane and held at +700 mV (a potential greater than the oxidation potential of DA) was used to measure DA flux through oxidation reactions. Amperometric currents in response to the addition of AMPH were recorded using an Axopatch 200B amplifier (Molecular Devices, Union City, CA) with a low-pass Bessel filter set at 1 kHz; traces were digitally filtered offline at 1 Hz using Clampex9 software (Molecular Devices, Union City, CA). DA efflux was quantified as the peak value of the amperometric current for all experiments except for recordings from *Drosophila* neurons. For *Drosophila* neurons, total DA efflux was quantified as the integral of the trace for a fixed 15 minute window. Dopaminergic neurons were recognized by fluorescence microscopy since the TH-GAL4 drives the expression of mCherry in dopaminergic neurons.

[^{3}H]DA uptake. Cells were plated on poly-D-lysine coated, 24-well plates and grown to ~90% confluence. On the day of the experiment, cells were washed once with 37°C KRH buffer

containing 10 mM dextrose, 100 µM pargyline, 1 mM tropolone, and 100 µM ascorbic acid, and equilibrated for 5 minutes at 37°C. Saturation kinetics of DA uptake was determined using a mixture of [^{3}H]DA (PerkinElmer Life Sciences, Waltham, MA) and unlabeled DA diluting to final DA concentrations of 0.01 µM - 10 µM. Uptake was initiated by bath addition of the dilution row mixture. Uptake was terminated after 10 minutes by washing twice in ice-cold KRH buffer. Scintillation fluid (Optiphase HiSafe 3, PerkinElmer Life Sciences) was added to the wells and the plates were counted in a Wallac Tri-Lux β-scintillation counter (Wallac). Nonspecific binding was determined in the presence of 10 µM cocaine. K_m and V_{max} values were derived by fitting Michaelis-Menten kinetics to the background corrected uptake data, using GraphPad Prism 5.0 (GraphPad Software, San Diego, CA). All determinations were performed in triplicates.

Computational Modeling. To evaluate the interactions between PIP$_2$-enriched membranes and the N-terminal region of the hDAT (residues 1-59), as well as the hDAT K/A and hDAT K/N mutants, molecular models were constructed with the knowledge-based structure-prediction tool Rosetta[40]. 1,000 different structures obtained from the structure prediction protocols in Rosetta were filtered through clustering according to a criterion of *maximization of common structure conservation* implemented in the in-house algorithm RMSDTT[41], which has been introduced into the molecular graphics program, visual molecular dynamics (VMD)[42]. Clusters with the largest numbers of conformations (usually 2−3 top clusters for each construct) were selected for further refinement with atomistic molecular dynamics (MD) simulations, to find the motifs within each cluster that were most frequently found in the Rosetta prediction. Predicted structures of the hDAT N-terminus, incorporating these most frequent motifs, were then subjected to both unbiased MD and replica exchange MD[43] simulations to assess the stability of the overall fold of the N-terminus, as well as of the individual structural elements identified with Rosetta.

The top structures that underwent the filtering process, described above, were further examined for suitability in the complete model of the hDAT transmembrane bundle (TMB)[26-28]. The

structures were embedded into a compositionally-asymmetric lipid membrane model (5:45:50 mixture of PIP$_2$/POPE (phosphatidylethanolamine) / POPC (phosphatidylcholine) on the intracellular leaflet, and 30:70 mixture of sphingomyelin / POPC on the extracellular leaflet[44]. Docking of the N-terminus (1-59 residues) to the TMB (residues 57-590) was carried out with Modeller[45]. Specific poses for the N-terminal constructs, relative to the TMB, were selected based on the criterion of positioning the largest positive electrostatic potential isosurfaces (EPIs) towards the membrane surface. As shown before[29], such configurations not only result in the strongest electrostatic interactions between the protein and the PIP$_2$-containing membrane, but also produce the highest levels of concomitant PIP$_2$ sequestration by the N-terminal peptide. These juxtamembrane poses of the N-terminus served as starting configurations for subsequent studies of the dynamics of PIP$_2$ lipids near the hDAT N-terminus, as detailed below.

The protocol used to evaluate the interaction of the hDAT N-terminus with PIP$_2$-containing membranes is based on the application of the self-consistent mean-field model (SCMFM) that evaluates the steady state distributions of charged lipid species (PIP$_2$, in this case) under the influence of electrostatic forces from a membrane-adsorbing macromolecule (here, the hDAT N-terminus) and quantifies the corresponding adsorption energies. As described in detail[29-31], the SCMFM is a mesoscale approach, based on the non-linear Poisson-Boltzmann (NLPB) theory of electrostatics[46] and Cahn-Hilliard dynamics[47], in which the protein is considered in 3-dimensional full atomistic detail, and the lipid membrane is considered as a 2-dimensional, tensionless, incompressible low-dielectric elastic slab in which the equilibrium distribution of different lipid species around adsorbing protein is obtained by self-consistent minimization. The governing free energy function contains contributions from electrostatic interactions, lipid mixing entropy, and mixing entropy of mobile salt ions in the solution. The SCMFM calculation of the membrane interaction of the hDAT N-terminus constructs (hDAT and the hDAT K/A or hDAT K/N mutants) considered in full atomistic detail (with partial charge and atomic radii taken from the all-atom CHARMM27 force field with CMAP corrections for proteins[48], was carried out with

the N-terminus positioned 2Å away from the lipid surface with average surface charge density of -0.0031e (corresponding to a lipid mixture with 5% PIP$_2$). The NLPB equation was then solved numerically as described[29-31], in a 0.1 M ionic solution of monovalent counterions (corresponding to λ=9.65Å Debye length), and using a dielectric constant of 2 for membrane interior and protein, and 80 for the solution.

AMPH Uptake. Plated hDAT, hDAT K/N, and hDAT K/A cells, as well as untransfected cells (to account for non-specific AMPH uptake) were washed with KRH assay buffer and incubated for 5 min at 37 °C with 10 nM AMPH. Cells were washed three times with ice-cold KRH and AMPH was extracted with acidic organic solvent. AMPH was quantified by reversed-phase HPLC using the Waters AccQ·Tag® method which uses pre-column derivatized reagents that help separate and easily detect fluorescence adducts (Waters Corporation, Milford, MA). AMPH uptake (with non-specific uptake subtracted) was normalized to hDAT levels and expressed as a percent.

Drosophila Genetics, Molecular Biology, and Construction of UAS hDAT. Flies lacking the *Drosophila* dopamine transporter (*DAT^{fmn}*)[35] and flies harboring TH-Gal4[49] were outcrossed to a control line (Bloomington Indiana (BI) 6326) and selected by PCR or by eye color. TH-GAL4 (BI 8848) and M{vas-int.Dm}ZH-2A, M{3xP3-RFP.attP'} ZH-22A (BI 24481) were obtained from the BI stock center and outcrossed to flies lacking the *Drosophila* DAT (*DAT^{fmn}*) and carrying the *white* (*w^{1118}*) mutation (BI stock number 6236) for 5–10 generations. Transgenes (hDAT or hDAT K/A) were cloned into pBI-UASC[50], and constructs were injected into embryos from M{vas-int.Dm}ZH-2A, M{3xP3-RFP.attP'}ZH-22A (BI 24481). Initial potential transformants were isolated by selecting for red eyes and lack of GFP signal in the head. Transformants were also verified by RFP fluorescence and outcrossed 5-8 times to *DAT^{fmn}* flies. The presence of *DAT^{fmn}* lesion was verified by PCR. Flies were maintained on a standard cornmeal/molasses/yeast media at 25°C and 65% humidity with a 12 hour/12hour light/dark cycle. Lights came on at 8 AM and off at 8 PM.

Behavioral Analysis. Three-day-old males were collected and placed into tubes with food for three days. After three days locomotion was recorded for 32 hours by beam breaks and analyzed using equipment/software from Trikinetics (www.trikinetics.com). For the AMPH-induced locomotion, males were starved for 6 hours and then fed sucrose (10 mM) containing either AMPH (1 mM) or vehicle.

Statistical Analysis. Compiled data are expressed as normalized mean values ± standard error. For statistical analysis, we used either a Student's t-test or one-way ANOVA depending on the n of the experimental groups. $P < 0.05$ was considered statistically significant.

References

1   Suh, B. C. & Hille, B. PIP2 is a necessary cofactor for ion channel function: how and why? *Annu Rev Biophys* 37, 175-195, doi:10.1146/annurev.biophys.37.032807.125859 (2008).

2   McLaughlin, S. & Murray, D. Plasma membrane phosphoinositide organization by protein electrostatics. *Nature* 438, 605-611, doi:10.1038/nature04398 (2005).

3   Kadamur, G. & Ross, E. M. Mammalian phospholipase C. *Annual review of physiology* 75, 127-154, doi:10.1146/annurev-physiol-030212-183750 (2013).

4   Czech, M. P. PIP2 and PIP3: complex roles at the cell surface. *Cell* 100, 603-606 (2000).

5   Ben-Aissa, K. *et al.* Activation of Moesin, a Protein That Links Actin Cytoskeleton to the Plasma Membrane, Occurs by Phosphatidylinositol 4,5-bisphosphate (PIP2) Binding Sequentially to Two Sites and Releasing an Autoinhibitory Linker. *The Journal of biological chemistry* 287, 16311-16323, doi:M111.304881 [pii]
10.1074/jbc.M111.304881.

6   Whorton, M. R. & MacKinnon, R. Crystal structure of the mammalian GIRK2 K+ channel and gating regulation by G proteins, PIP2, and sodium. *Cell* 147, 199-208, doi:S0092-8674(11)00997-4 [pii]
10.1016/j.cell.2011.07.046.

7   Buchmayer, F. *et al.* Amphetamine actions at the serotonin transporter rely on the availability of phosphatidylinositol-4,5-bisphosphate. *Proceedings of the National Academy of Sciences of the United States of America* 110, 11642-11647, doi:10.1073/pnas.1220552110 (2013).

8   Pizzo, A. B. *et al.* The membrane raft protein Flotillin-1 is essential in dopamine neurons for amphetamine-induced behavior in Drosophila. *Molecular psychiatry* 18, 824-833, doi:10.1038/mp.2012.82 (2013).

9   Hamilton, P. J. *et al.* De novo mutation in the dopamine transporter gene associates dopamine dysfunction with autism spectrum disorder. *Molecular psychiatry*, doi:10.1038/mp.2013.102 (2013).
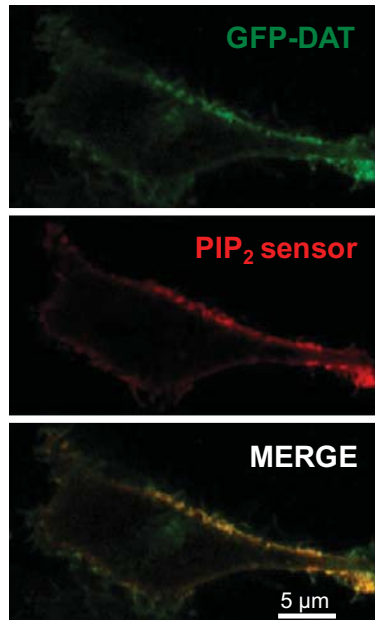
10   Giros, B., Jaber, M., Jones, S. R., Wightman, R. M. & Caron, M. G. Hyperlocomotion and indifference to cocaine and amphetamine in mice lacking the dopamine transporter. *Nature* 379, 606-612 (1996).

11   Sulzer, D., Sonders, M. S., Poulsen, N. W. & Galli, A. Mechanisms of neurotransmitter release by amphetamines: a review. *Prog Neurobiol* 75, 406-433 (2005).

12   Robertson, S. D., Matthies, H. J. & Galli, A. A closer look at amphetamine-induced reverse transport and trafficking of the dopamine and norepinephrine transporters. *Mol Neurobiol* 39, 73-80, doi:10.1007/s12035-009-8053-4 (2009).

13   Cervinski, M. A., Foster, J. D. & Vaughan, R. A. Psychoactive substrates stimulate dopamine transporter phosphorylation and down regulation by cocaine sensitive and protein kinase C dependent mechanisms. *The Journal of biological chemistry* (2005).

14   Khoshbouei, H. *et al.* N-terminal phosphorylation of the dopamine transporter is required for amphetamine-induced efflux. *PLoS Biol* 2, E78 (2004).

15   Fog, J. U. *et al.* Calmodulin kinase II interacts with the dopamine transporter C terminus to regulate amphetamine-induced reverse transport. *Neuron* 51, 417-429 (2006).

16   Cremona, M. L. *et al.* Flotillin-1 is essential for PKC-triggered endocytosis and membrane microdomain localization of DAT. *Nature neuroscience* 14, 469-477, doi:nn.2781 [pii]
10.1038/nn.2781 (2011).

17   Wang, J. & Richards, D. A. Segregation of PIP2 and PIP3 into distinct nanoscale regions within the plasma membrane. *Biology open* 1, 857-862, doi:10.1242/bio.20122071 (2012).

18   Hope, H. R. & Pike, L. J. Phosphoinositides and phosphoinositide-utilizing enzymes in detergent-insoluble lipid domains. *Mol Biol Cell* 7, 843-851 (1996).

19   Varnai, P. & Balla, T. Visualization of phosphoinositides that bind pleckstrin homology domains: calcium- and agonist-induced dynamic changes and relationship to myo-[3H]inositol-labeled phosphoinositide pools. *J Cell Biol* 143, 501-510 (1998).

20   McLaughlin, S., Wang, J., Gambhir, A. & Murray, D. PIP(2) and proteins: interactions, organization, and information flow. *Annual review of biophysics and biomolecular structure* 31, 151-175, doi:10.1146/annurev.biophys.31.082901.134259 (2002).

21   Hilgemann, D. W. & Ball, R. Regulation of cardiac Na+,Ca2+ exchange and KATP potassium channels by PIP2. *Science* 273, 956-959 (1996).

22   Bowton, E. *et al.* Dysregulation of dopamine transporters via dopamine D2 autoreceptors triggers anomalous dopamine efflux associated with attention-deficit hyperactivity disorder. *The Journal of neuroscience : the official journal of the Society for Neuroscience* 30, 6048-6057, doi:30/17/6048 [pii]
10.1523/JNEUROSCI.5094-09.2010 (2010).

23   Binda, F. *et al.* Syntaxin 1A interaction with the dopamine transporter promotes amphetamine-induced dopamine efflux. *Mol Pharmacol* 74, 1101-1108 (2008).

24   Varnai, P. *et al.* Inositol lipid binding and membrane localization of isolated pleckstrin homology (PH) domains. Studies on the PH domains of phospholipase C delta 1 and p130. *The Journal of biological chemistry* 277, 27412-27422, doi:10.1074/jbc.M109672200
M109672200 [pii] (2002).

25   Robbins, J., Marsh, S. J. & Brown, D. A. Probing the regulation of M (Kv7) potassium channels in intact neurons with membrane-targeted peptides. *The Journal of neuroscience : the official journal of the Society for Neuroscience* 26, 7950-7961, doi:26/30/7950 [pii]
10.1523/JNEUROSCI.2138-06.2006 (2006).

26   Beuming, T. *et al.* The binding sites for cocaine and dopamine in the dopamine transporter overlap. *Nature neuroscience* 11, 780-789 (2008).

27   Bisgaard, H. *et al.* The binding sites for benztropines and dopamine in the dopamine transporter overlap. *Neuropharmacology* 60, 182-190, doi:10.1016/j.neuropharm.2010.08.021 (2011).

28   Kniazeff, J. *et al.* An intracellular interaction network regulates conformational transitions in the dopamine transporter. *The Journal of biological chemistry* 283, 17691-17701, doi:10.1074/jbc.M800475200 (2008).

29   Khelashvili, G., Galli, A. & Weinstein, H. Phosphatidylinositol 4,5-biphosphate (PIP(2)) lipids regulate the phosphorylation of syntaxin N-terminus by modulating both its position and local structure. *Biochemistry* 51, 7685-7698, doi:10.1021/bi300833z (2012).

30   Khelashvili, G., Harries, D. & Weinstein, H. Modeling membrane deformations and lipid demixing upon protein-membrane interaction: the BAR dimer adsorption. *Biophysical journal* 97, 1626-1635, doi:10.1016/j.bpj.2009.07.006 (2009).

31   Khelashvili, G., Weinstein, H. & Harries, D. Protein diffusion on charged membranes: a dynamic mean-field model describes time evolution and lipid reorganization. *Biophysical journal* 94, 2580-2597, doi:10.1529/biophysj.107.120667 (2008).

32   Balla, T., Szentpetery, Z. & Kim, Y. J. Phosphoinositide signaling: new tools and insights. *Physiology (Bethesda)* 24, 231-244, doi:24/4/231 [pii]
10.1152/physiol.00014.2009 (2009).

33   Wicker-Thomas, C. & Hamann, M. Interaction of dopamine, female pheromones, locomotion and sex behavior in Drosophila melanogaster. *J Insect Physiol* 54, 1423-1431, doi:S0022-1910(08)00159-5 [pii]
10.1016/j.jinsphys.2008.08.005 (2008).

34   Pendleton, R. G., Rasheed, A., Sardina, T., Tully, T. & Hillman, R. Effects of tyrosine hydroxylase mutants on locomotor activity in Drosophila: a study in functional genomics. *Behav Genet* 32, 89-94 (2002).

35   Kume, K., Kume, S., Park, S. K., Hirsh, J. & Jackson, F. R. Dopamine is a regulator of arousal in the fruit fly. *The Journal of neuroscience : the official journal of the Society for Neuroscience* 25, 7377-7384, doi:25/32/7377 [pii]
10.1523/JNEUROSCI.2048-05.2005 (2005).

36   van Rheenen, J., Achame, E. M., Janssen, H., Calafat, J. & Jalink, K. PIP2 signaling in lipid domains: a critical re-evaluation. *The EMBO journal* 24, 1664-1673, doi:10.1038/sj.emboj.7600655 (2005).

37   Sorkina, T., Caltagarone, J. & Sorkin, A. Flotillins regulate membrane mobility of the dopamine transporter but are not required for its protein kinase C dependent endocytosis. *Traffic* 14, 709-724, doi:10.1111/tra.12059 (2013).

38   Gabriel, L. R. *et al.* Dopamine transporter endocytic trafficking in striatal dopaminergic neurons: differential dependence on dynamin and the actin cytoskeleton. *The Journal of neuroscience : the official journal of the Society for Neuroscience* 33, 17836-17846, doi:10.1523/JNEUROSCI.3284-13.2013 (2013).

39   Mazei-Robison, M. S. *et al.* Anomalous dopamine release associated with a human dopamine transporter coding variant. *The Journal of neuroscience : the official journal of the Society for Neuroscience* 28, 7040-7046, doi:28/28/7040 [pii]
10.1523/JNEUROSCI.0473-08.2008 (2008).

40   Das, R. & Baker, D. Macromolecular modeling with rosetta. *Annual review of biochemistry* 77, 363-382, doi:10.1146/annurev.biochem.77.062906.171838 (2008).

41   Gracia, L. *RMSDTT: RMSD Trajectory Tool, 2.5 ed.*, (2005).

42   Humphrey, W., Dalke, A. & Schulten, K. VMD: visual molecular dynamics. *Journal of molecular graphics* 14, 33-38, 27-38 (1996).

43   Earl, D. J. & Deem, M. W. Parallel tempering: theory, applications, and new perspectives. *Physical chemistry chemical physics : PCCP* 7, 3910-3916 (2005).

44   Kiessling, V., Wan, C. & Tamm, L. K. Domain coupling in asymmetric lipid bilayers. *Biochimica et biophysica acta* 1788, 64-71, doi:10.1016/j.bbamem.2008.09.003 (2009).
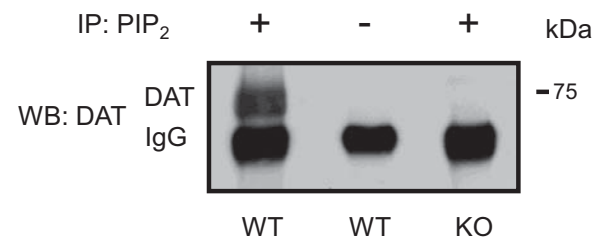
45   Sali, A. & Blundell, T. L. Comparative protein modelling by satisfaction of spatial restraints. *Journal of molecular biology* 234, 779-815, doi:10.1006/jmbi.1993.1626 (1993).

46   Sharp, K. A. & Honig, B. Electrostatic interactions in macromolecules: theory and applications. *Annual review of biophysics and biophysical chemistry* 19, 301-332, doi:10.1146/annurev.bb.19.060190.001505 (1990).

47   Chaikin, P. M. & Lubensky, T. C. *Principles of Condensed Matter Physics*. (Cambridge university press, 2000).

48   Mackerell, A. D., Jr., Feig, M. & Brooks, C. L., 3rd. Extending the treatment of backbone energetics in protein force fields: limitations of gas-phase quantum mechanics in reproducing protein conformational distributions in molecular dynamics simulations. *Journal of computational chemistry* 25, 1400-1415, doi:10.1002/jcc.20065 (2004).

49   Friggi-Grelin, F. *et al.* Targeted gene expression in Drosophila dopaminergic cells using regulatory sequences from tyrosine hydroxylase. *Journal of neurobiology* 54, 618-627, doi:10.1002/neu.10185 (2003).

50   Wang, J. W., Beck, E. S. & McCabe, B. D. A modular toolset for recombination transgenesis and neurogenetic analysis of Drosophila. *PloS one* 7, e42102, doi:10.1371/journal.pone.0042102 (2012).
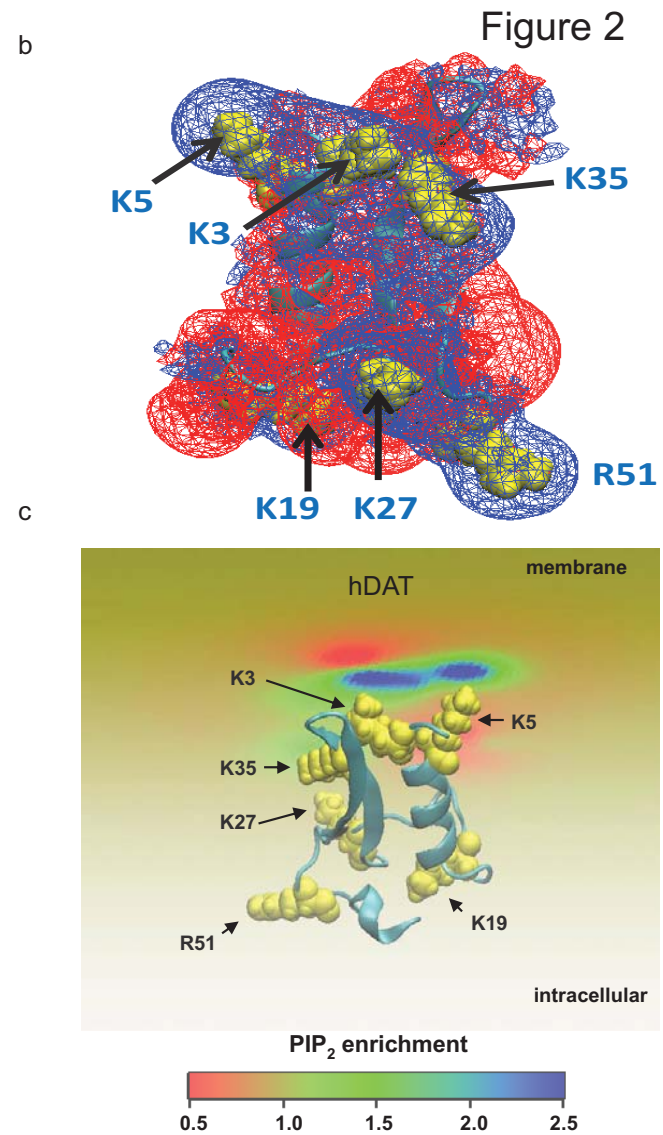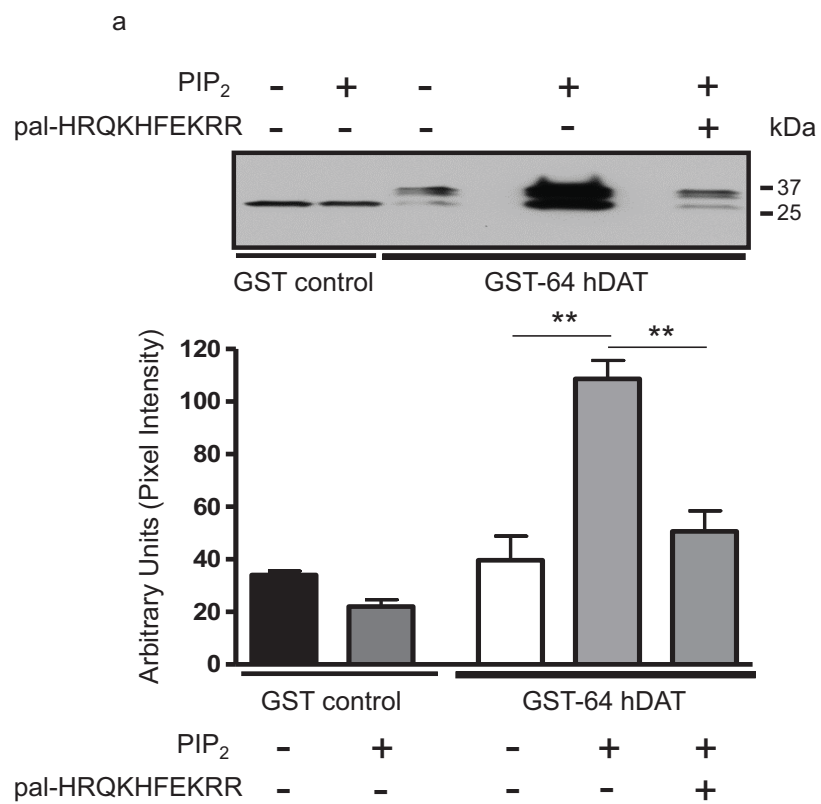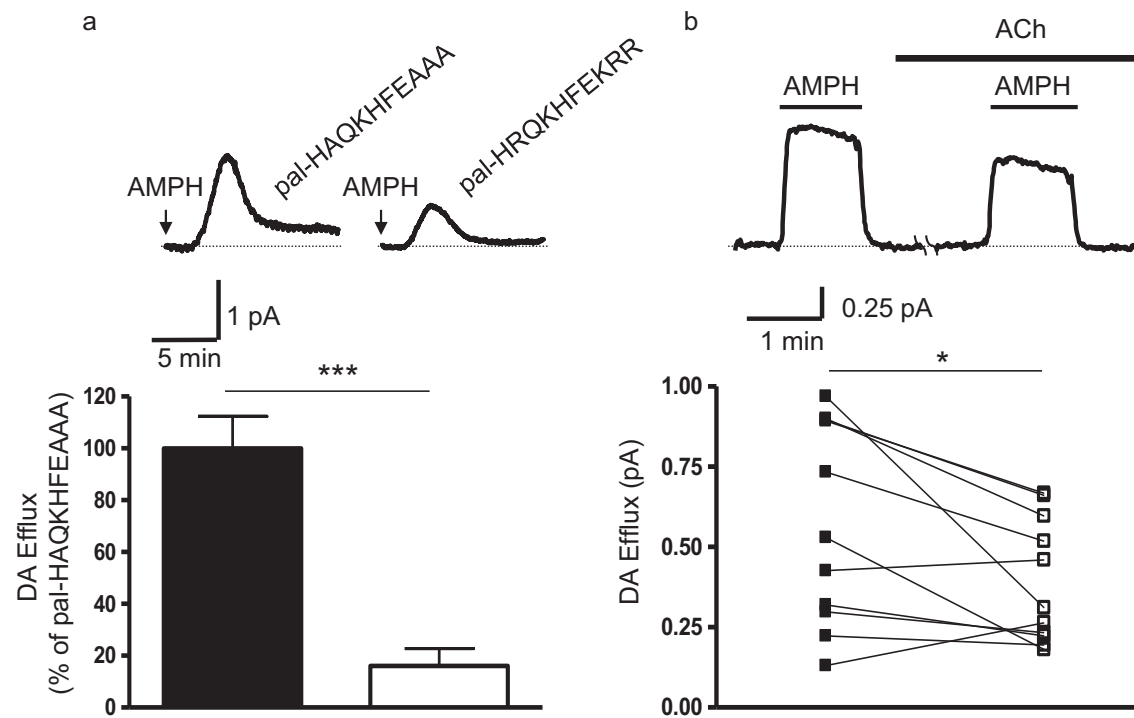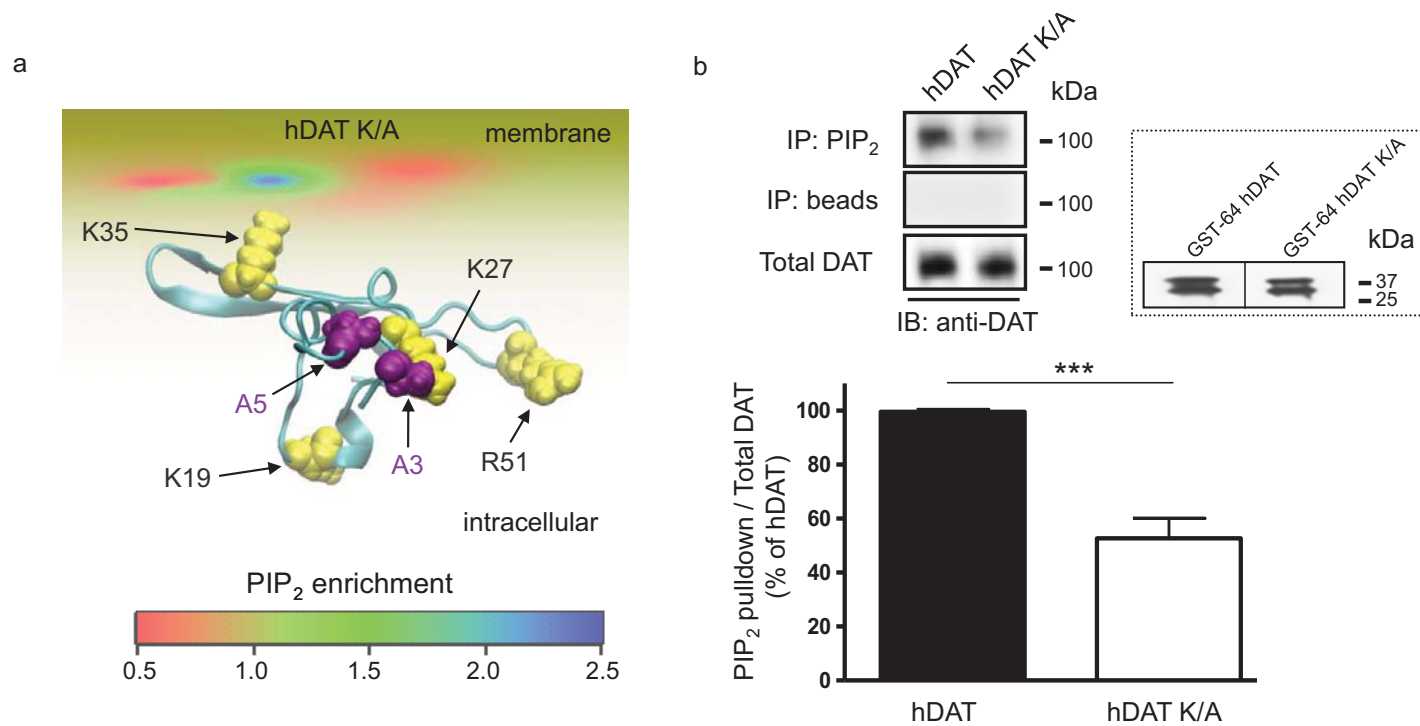
Figure 1

a

GFP-DAT

PIP$_2$ sensor

MERGE

5 μm

b

IP: PIP$_2$ +   −   +   kDa

WB: DAT DAT

IgG   −75

WT   WT   KO

Figure 2

a

PIP$_2$ −   +   −   +   +
pal-HRQKHFEKRR   −   −   −   −   +   kDa

GST control   GST-64 hDAT

b

K5   K3   K35   K19   K27   R51

c

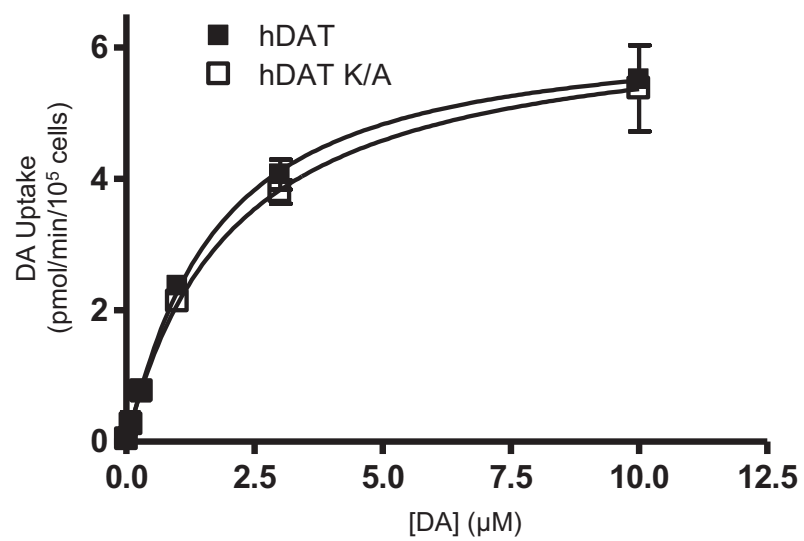hDAT   membrane

K3   K5   K35   K27   R51   K19

intracellular

PIP$_2$ enrichment

0.5   1.0   1.5   2.0   2.5

Figure 3

Figure 4

Figure 5

Figure 6

a

b

Figure 7